Title
A Chiral Microcavity based on Apparent Circular Dichroism

Authors
Tzu-Ling Chen,[1,2,6] Andrew Salij,[3,6] Katherine A. Parrish,[1,6] Julia K. Rasch,[1] Francesco Zinna,[4] Paige J. Brown,[3] Gennaro Pescitelli,[4] Francesco Urraci,[4] Laura A. Aronica,[4] Abitha Dhavamani,[5] Michael S. Arnold,[5] Michael R. Wasielewski,[3] Lorenzo di Bari,[4] Roel Tempelaar,[3*] Randall H. Goldsmith[1*]

Affiliations
[1]Department of Chemistry, University of Wisconsin-Madison, [2]Department of Photonics, National Yang Ming Chiao Tung University, [3]Department of Chemistry, Northwestern University, [4] Dipartimento di Chimica e Chimica Industriale, Università di Pisa, [5]Department of Materials Science and Engineering, University of Wisconsin-Madison, [6]These authors contributed equally to this work.

Abstract

Breaking the symmetry between left-handed and right-handed chiral optical modes in planar Fabry–Pérot (FP) microcavities would enable a variety of chiral light-matter phenomena, with applications in spintronics, polaritonics, and chiral lasing. Such symmetry breaking, however, has remained underexplored and has been purported to require Faraday mirrors. We present a simple solution to chiral symmetry breaking in FP microcavities, preserving low mode volumes by embedding organic thin films exhibiting "apparent circular dichroism" (ACD); an optical phenomenon based on interfering linear birefringence and linear dichroism with offset optical axes. ACD interactions are opposite for counter-propagating light and increase with path length. Consequently, we demonstrated chiral asymmetry of the cavity modes over an order of magnitude larger than that of the isolated thin film. Through both circular dichroism spectroscopy and simulation using theoretical scattering matrix methods, we characterize the spatial, spectral, and angular chiroptical responses of this new type of chiral microcavity.

Introduction
Chirality, a fundamental property found in nature, has significant implications in many scientific and technological fields. [1] Chiral molecules and materials exhibit unique interactions with light, enabling matter to discriminate between the spin angular momenta of photons. This feature has led to growing interest in quantum control of chiral degrees of freedom for quantum information science (QIS), resulting in the exploration of techniques for manipulating electron spins,[2] constructing spin filters,[3] observing the chiral Purcell effect,[4] developing chiral-induced spin selectivity,[5] and developing quantum information storage and processing.[6,7] Moreover, the advancement of circularly polarized luminescent (CPL) materials shows the ability to generate

circular polarized light, leading to promising applications, including displays, optical sensing, and optical data storage.[8]

Efficient transduction of chiral polarizations between light and matter requires both strong light-matter coupling and high discrimination between left-handed and right-handed circularly polarized (LCP and RCP) light. In recent years, planar Fabry-Pérot (FP) microcavities with small mode volumes have received increasing attention as a straightforward means of reaching the strong-coupling regime by allowing multiple round trips between two mirrors in the resonant modes of the cavity, resulting in a longer effective interaction length of light with the embedded material. Through this mechanism, FP microcavities support photon-matter hybrid excitations known as polaritons, with diverse applications in condensed matter physics, quantum materials, and chemical reaction dynamics.[9–13] While FP cavities can sustain chiral modes featuring well-defined circular motion of local field amplitudes,[14] and such angular motion can in principle induce angular momentum states in non-centrosymmetric samples such as monolayer transition-metal dichalcogenides,[15] such cavities by themselves do not discriminate between chiral optical modes. For that reason, there is a significant interest in breaking the chiral symmetry of FP microcavities in order to produce chiral microcavities. Here, we describe a new and accessible strategy for producing planar FP microcavities that exhibit a strong chiral asymmetry.

However, standard optical cavities cannot break chiral symmetry when samples exhibiting natural optical activity are embedded because the handedness of circularly polarized light is reversed upon each reflection. Though samples exhibiting natural optical activity offer a source of dissymmetry, they do not couple asymmetrically to the locally-rotating chiral fields in FP microcavities. Consequently, such locally-rotating fields that correspond to an opposite handedness for counterpropagating light require embedded materials with a chiroptical response that is *inverted* for opposite irradiation directions. Materials with a chiral response traditionally exhibit invariance with respect to their orientation, meaning that their interaction with LCP and RCP light is independent of the direction of light propagation (unless electric or magnetic fields are applied). Hence, in addition to being time reversible, natural optical activity is Lorentz reciprocal. Furthermore, the sign of the chiroptical response remains invariant upon flipping the sample orientation, described as directional reciprocity [16]. Natural optical activity obeying both forms of reciprocity is understood as deriving from a static angle between the transition electric and magnetic dipole moments in the plane of polarization [17]. As a result, simply embedding chiral molecules will not make a chiral cavity.

A variety of efforts have focused on control of chirality in photonic structures. For macroscopic cavities, the breaking of chiral symmetry can be realized through the use of Faraday rotators [18] or different, non-FP, cavity geometries such as ring cavities [14], methods that are not conducive for use with microcavities. Inclusion of matched quarter waveplates inside a macroscopic cavity can enable the accumulation and sensing of optical rotation, but are not compatible with use of a microcavity, while the intracavity fields are predominantly linear or helicoidal, which may not be conducive for chiral polariton formation [19,20]. Chiral plasmonic structures or metamaterials [21–24] can prevent inversion of chirality upon reflection or magnify local chiral fields, enabling breakthroughs in the efficient manipulation of chiral light emission [25] and interaction with chiral molecules [26,27], but these structures can be lossy and/or difficult to fabricate. Recent advancements in nanomaterials technology have enabled the enhancement of chiral signals originating from

small-molecule chirality through self-assembly and chiral nanostructures, achieving CD levels in the sub-degree range [28–34]. In a recent study, the necessary conditions for chiral symmetry breaking in FP microcavities were realized based on a planar chiral film under torsional shear stress [35], but this symmetry breaking only affected modes with significant polarization in the cavity plane (i.e., propagation direction far from normal incidence), complicating incorporation of such materials into photonic quantum interfaces and implementation of transduction schemes.

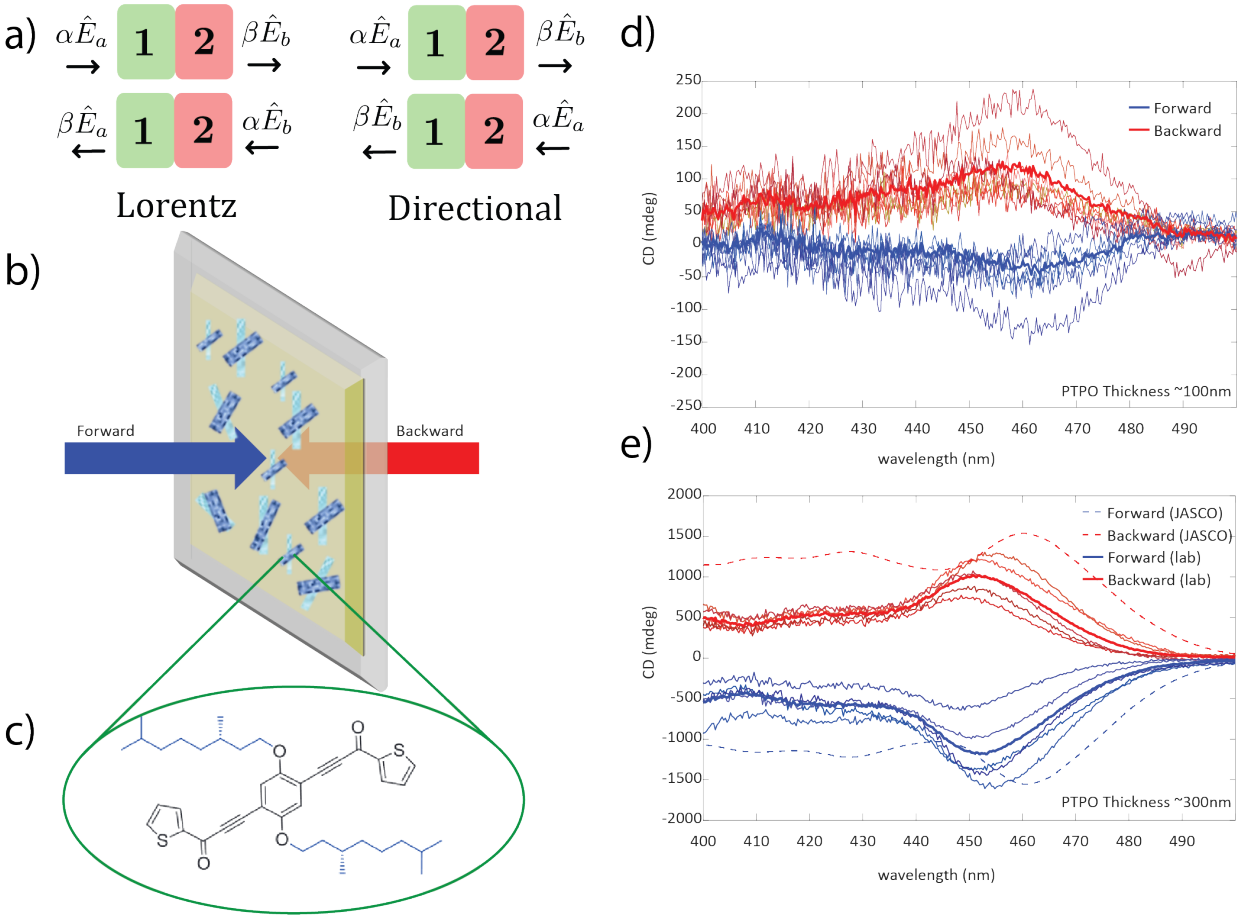

Fig.1 Chiroptical properties and signal inversion (directionally non-reciprocal features) of PTPO films. (a) Symmetry relations and comparison of Lorentz (signal is invariant to an interchange of light source and detector) and directional (signal is invariant to an interchange of propagation direction) reciprocity. Vectors designated with magnitudes given by α, β and unit polarizations of subscripts a and b. Numbering and coloring indicated to order sample along a unique orientation. b) Sample geometry of PTPO film on an HR substrate. c) Structure of PTPO. d-e) Chiroptical properties of 100 nm (d) and 300 nm (e) PTPO film on an HR substrate measured at different spatial locations. Blue curves are acquired in the forward geometry (see b) and red curves are acquired in the backwards geometry. The thick solid curves show the average from several different spots in the backward or forward direction. Plots in d) were obtained using a homebuilt CD spectrometer. Plots labeled "lab" in e) were also acquired on the homebuilt spectrometer. Plot e) also includes characterization of the same film with a commercial spectrometer (JASCO-1500), which shows qualitative agreement with laboratory-measured samples.

New options for creating chiral microcavities can derive from new materials featuring chiral π-conjugated oligothiophenes that obey Lorentz reciprocity, but *not* directional reciprocity, leading to unusual chiroptical responses that result in signal inversion upon sample flipping [36], Figure 1a. During the fabrication process, the oligothiophenes form thin films with a preferential orientation on a substrate as the chiral conjugated sidechains anneal and self-assemble into ordered crystals. These films demonstrate signal inversion of the handedness of the circularly polarized component preferentially absorbed by the two opposite faces of the sample [37,38], as shown in Figure 1. This property is due to "apparent" circular dichroism (ACD), which does not intrinsically originate at the molecular or microscopic level as in the case of natural optical activity, but rather originates from macroscopic ordering due to nonparallel axes of linear dichroism and linear birefringence, which occurs in oriented, low symmetry systems [39–41]. We also note that ACD should not be confused with the similarly-named anisotropic CD [42,43]. ACD possesses Lorentz reciprocity but categorically lacks that of directional reciprocity, Figure 1a, which offers the opportunity to induce directionally dependent polarization rotation, thus overcoming the critical limitation in microcavities that prevents amplification since this symmetry breaking counteracts the inversion of circular polarization of normal mirrors. Thus, ACD offers the ability to simply engineer chiral symmetry breaking in planar FP microcavities.

Despite its potential for breaking the symmetry between chiral modes in a FP microcavity, ACD has yet to be used to such an effect. Here, we demonstrate the usage of ACD to alter the chiral response of a microcavity by embedding a self-assembled chiral thin film [38], (S,S)-PTPO, 3,3'-(2,5-bis(((S)-3,7- dimethyloctyl)oxy)-1,4-phenylene)bis(1-(thiophen-2-yl)prop-2-yn-1-one), Figure 1b, c. PTPO films exhibit ACD, as evidenced by the shift in CD as a function of sample orientation, Figure 1d,e. To form a microcavity, two highly reflective (HR) mirrors, a chiral thin film of PTPO, and a transparent polymer binding layer (polyvinyl acetate, PVA) are combined, Figure 2a. Importantly, not only does this structure involve a broken symmetry between LCP and RCP modes, the chiroptical signal at the cavity resonance is an order of magnitude larger than that of the chiral thin film outside of the cavity. This phenomenon is the result of ACD signals being amplified upon experiencing an increased optical pathlength within the cavity environment.

Results

Characterization of films and microcavities

The CD spectra were obtained using a white light source and a home-built broadband spectroscopy platform where the LCP and RCP are generated by a quarter wave plate with two different angles to the fast-axis, as depicted in Figure 2b. Illumination is provided by the collimated output from a stabilized tungsten-halogen light source, which is focused on a target for measuring the transmission spectra, see Materials and Methods. For every measurement, the background spectra of LCP and RCP with no sample is verified to be equal, ensuring that the signal is solely due to the sample. CD spectra were recorded on the same films in forward (PVA-coated side facing the HR mirror, Figure 2a)) and backward configuration. CD, measured in millidegrees (mdeg), is defined as [44]

$$CD = 32980 * log_{10} \frac{I_R}{I_L} \qquad (1)$$

where $I_{R(L)}$ denotes the intensity of transmitted RCP (LCP) light.

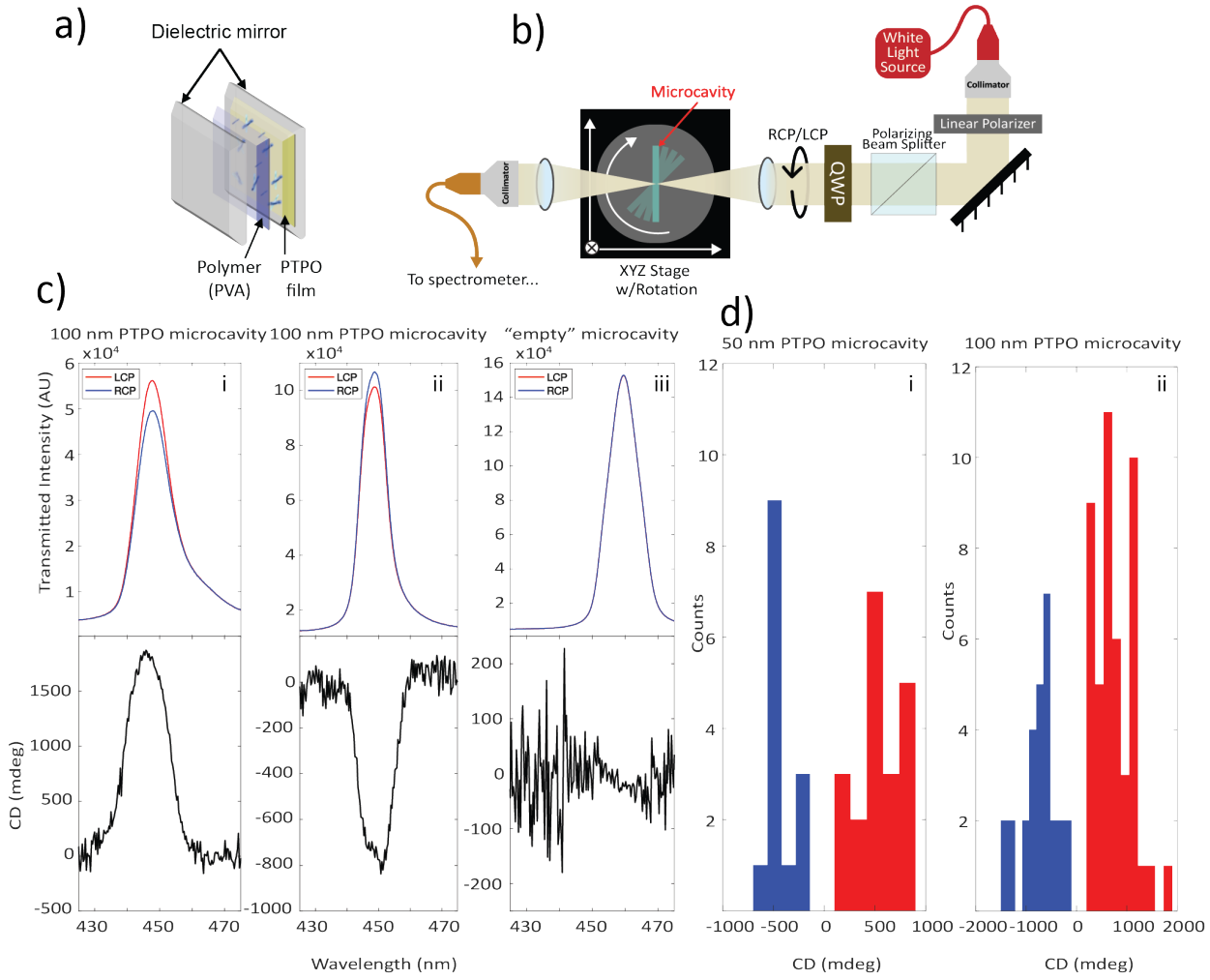

Fig. 2 Chiral microcavity configuration and demonstration of microcavity chiroptical response. (a) A schematic illustration of the FP microcavity architecture used in our experiments. (b) A single-beam white light system that directs the cavity transmission signal to a spectrometer. The quarter-wave plate (QWP) generates RCP and LCP. A rotational stage is employed to provide angular dispersion of the microcavity spectrum. (c) Transmitted intensities of RCP (red) and LCP (blue), on top, and calculated CD in mdeg (black) for the same spectral regions. (i, ii) are two different PTPO microcavities while (iii) is a microcavity with no PTPO. (d) CD values measured over a variety of microcavities and microcavity positions for a (i) 50 nm thick PTPO film and a (ii) 100 nm thick PTPO film.

Isolated chiral thin films exhibiting ACD

To inspect the directionally nonreciprocal features of the PTPO, thin films were deposited on a HR substrate with 95% reflectivity (Evaporated Coatings Inc, Figure S1), the same that will ultimately be used to assemble the microcavity, Figure 1b. The HR substrates were coated with

three different thicknesses of PTPO: 300 nm, 100 nm, and 50 nm. Chiral signals from the 100 nm thick films were weaker than the 300 nm films, though a clear difference between LCP and RCP excitation emerges, resulting in a non-zero value of CD, Figure 1d. The maximum CD values of 100-200 mdeg is near 455 nm. The value of CD is also opposite in the forward and backward configurations, which shows distinct evidence for the directional non-reciprocity property of the chiral thin film and is consistent with previous measurement [38]. For 300 nm films, CD spectra are easily quantified and also show directional non-reciprocity, Figure 1e. The behavior of samples measured with the home-built spectrometer also tracks values acquired with a commercial CD spectrometer on the same HR substrate. From comparison between CD values of the 100 and 300 nm thin films, the maximum CD value is observed to increase by roughly a factor of ten when the thin film triples in length. This behavior is qualitatively consistent with ACD's theoretical quadratic dependence on pathlength [41], though such dependence is limited by mean absorption and higher order Mueller matrix polarization effects [15], and differences in molecular ordering, as further discussed below, will also play a role [45]. In addition to merely having a lower signal to noise ratio than the 300 nm film, the 100 nm film acts as a less effective chiral absorber per unit length. The CD spectrum of the 50 nm films are too small to measure on an HR substrate without more advanced techniques. Enhancing the comparatively weak signal of the 100 nm and 50 nm films using microcavities in the following section represents one of the core results of this investigation.

Experimental demonstration of a microcavity with asymmetric chiroptic response

In PTPO films deposited on HR substrates, a directionally nonreciprocal feature at the PTPO absorption band was observed at the range of 400-500 nm. It is anticipated that this feature will be amplified in a FP microcavity, where the reflectivity of the HR microcavity mirrors plays a significant role in determining the degree of temporal confinement and the linewidth of the cavity mode. These parameters are commonly expressed via the cavity finesse (F), which, in the limit of negligible internal cavity loss, is given by $F = \frac{\pi}{-ln(R)}$, where R corresponds to the reflectivity of the mirrors [46]. To demonstrate the cavity-enhanced chiroptic properties of the chiral thin film, planar FP microcavities were fabricated. These microcavities contain the chiral PTPO thin film between two mirrors and are configured as shown in Figure 2a. The absorption spectrum of the original PTPO thin film extends below 500 nm (2.48 eV) and the spectral range of the HR mirror coating (with the reflectance over 95%) is optimized between 440 and 500 nm. By adjusting the PVA thickness [47], the resonance peak was optimized and tuned to occur within the high reflectivity window.

Typical cavity transmission spectra and CD values from chiral microcavities (HR/100 nm PTPO/160 nm PVA/HR, see details in Material and Methods) are shown in Figure 2c(i,ii), and demonstrates a conspicuous difference between RCP and LCP light. In contrast, an empty microcavity with no PTPO film, but instead with a thicker PVA film (HR/260 nm PVA/HR), displays no discernible difference between RCP and LCP transmission, Figure 2c(iii). The cavity-enhanced CD value in the chiral microcavity encompasses the contribution of the chiroptical response from the chiral PTPO thin film and the enhancement provided by the microcavity. Both quantities are expected to be affected by the strength of the thin film absorption, with the chiroptic response positively correlated and the enhancement negatively correlated to it. After amplification in the FP microcavity, the CD value magnitude varies as function of sample and spot location,

reaching to nearly 1000 mdeg for 50 nm films and to nearly 2000 mdeg for 100 nm films, Figure 2d. These values are significantly larger than the CDs of the thin film on the HR substrate, which is less than 200 mdeg for the 100 nm film and unquantifiable for the 50 nm film, Figure 1d,e. Scatter exists in the CD values, indicating spatial variations of the CD of the thin film as well as the microcavity finesse, as discussed next.

Comparing Figure 1d with Figure 2d(ii) demonstrates that highest CD magnitudes for 100 nm PTPO microcavities are ~10-20x higher than the values measured for thin films of comparable thickness, though this comparison is inherently qualitative since the same thin film spot cannot be measured before and after microcavity construction. These same microcavities display finesse values of 30-45 (see Figure S2). The cavity finesse can be defined as 2π multiplied by the number of round trips before decay to 1/e of the initial optical intensity. Since each round trip includes two passes through the PTPO film, this simple analysis predicts enhancements of 10-14x, in qualitative agreement with the analysis above. Further analysis utilizing a side-mode resonance as an internal calibration for spot-to-spot variations of the intrinsic thin film CD value shows that the enhancement of the chiroptic response increases with finesse, which is consistent with a linear fit of the microcavity enhancement to optical pathlength (Figures S3 and S4, and Supplementary Information, SI). At optical path lengths of multiple cavity round trips, the expected theoretical pathlength dependence of CD diverges from the quadratic short pathlength regime [36] and approaches a linear regime, consistent with the empirically observed linear behavior. The clear chiroptic signals of the microcavity demonstrates two key results: that the PTPO film can generate a clear asymmetric chiral response in the microcavity, and that the microcavity can provide significant amplification to enhance the film's intrinsic directionally non-reciprocal properties.

Cavity angular dispersion

For a single microcavity, one can tune the resonant wavelength by changing the incident angle of radiation and therefore the photonic wavevector in the plane of the cavity [48]. Understanding this angular dependence is critical for elucidating the mechanism of chiroptic enhancement as well as evaluating the applicability of the microcavity for creation of polaritons and other applications in QIS [49]. To adjust the resonance wavelength of the cavity, the microcavities are placed on a precision rotation and translation stage for measurements at oblique incident angles, as shown in Figure 2b. As the angle of incidence deviates from the normal direction, the resonant peak of the cavity shifts towards lower wavelengths as anticipated from photonic angular dispersion. The cavity confines the resonant wave vectors perpendicular to the surface k_z while the parallel component $k_{||}$ remains free, resulting in a total energy blueshift that is reminiscent of a light-line.

When tuning the resonant wavelength of the chiral cavity, an intriguing trend emerges at the major microcavity resonance near 440 nm, where the CD value is higher at oblique incidence than at normal incidence, Figure 3 a,b. Multiple phenomena may contribute to this trend including properties of the film and spurious signals due to the microcavity, Figure 3c and Figure S5. For the film, one potential contribution is due to the shifting of resonant wavelengths into spectral regions where the ACD response of PTPO may vary. However, the ACD spectra for bare films, Figure 1d,e, is largely constant within the accessible range of the major cavity resonance (~440-450 nm). In addition, more minor spectral features are observed at higher wavelengths, Figure S3. The HR mirrors, which consist of distributed Bragg reflectors (DBR)s, support multiple

resonances in the spectral region of ACD for PTPO, resulting in multiple modes in the cavity ensemble. Increasing incident angle also increases the pathlength through the thin film, increasing the effective interaction distance, though this effect may be counteracted by a concomitant decrease in cavity finesse. A more quantitative analysis is presented below.

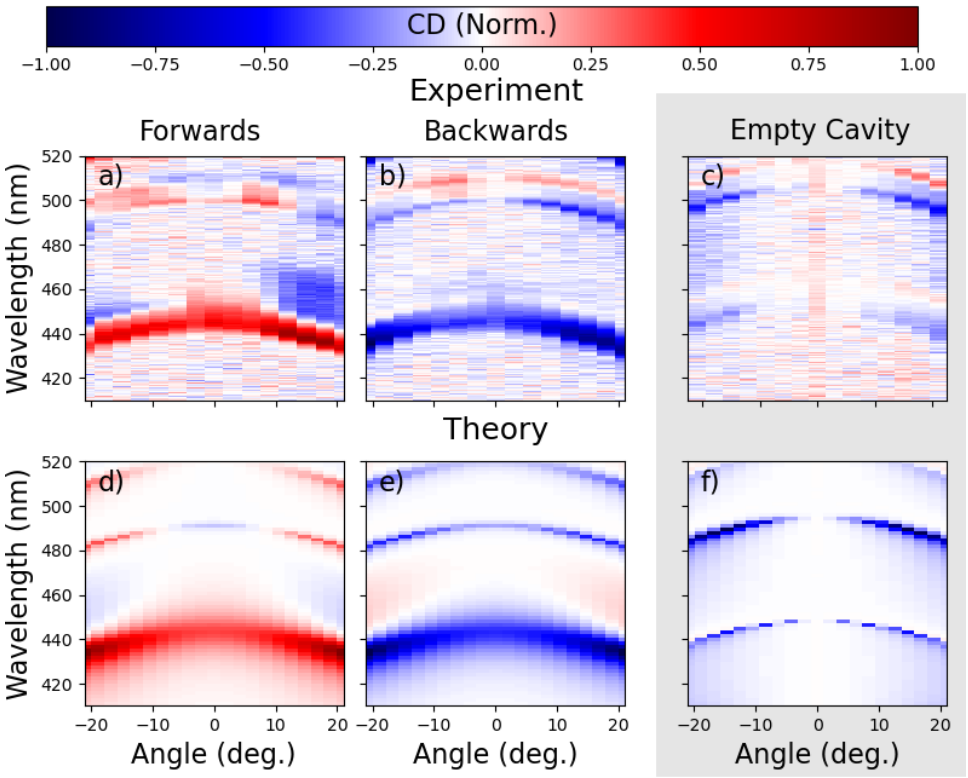

Figure 3. Angular and wavelength-dependent response of CD (normalized) for microcavity containing 100 nm PTPO. a,b) Experimental results for forwards and backwards propagation and contrasted c) empty cavity signals. d,e) Theoretical SMM results for forwards and backwards propagation alongside f) an empty cavity, see SI for details. Signals normalized to region of maximum magnitude of CD, which is roughly equivalent for forwards and backwards propagation but moderately weaker in the empty cavity.

Theoretical model comparison with experiment

While many implementations of microcavities often contain an isotropic and/or dilute matter component between the mirrors that interacts with the light, here the matter is a thin film that is both oriented and in the solid state. As such, behaviors such as interface effects and interference within the film become relevant, necessitating an approach that properly incorporates Maxwell's equations for multiple layers of media in order to understand how tuning the incident light wavevector into the cavity changes the response. To quantitatively describe the CD exhibited by the thin film at various angles, the CD signal for typical solid-state samples is expressed as follows[37]:

$$\mathrm{CD_{abs}} = \mathrm{CD_{iso}} + \frac{\mathrm{LD'\cdot LB - LD\cdot LB}}{2} + \mathrm{LB_{res}} \quad (1)$$

where CD_{iso}, LD, and LB represent the intrinsic isotropic component of the circular dichroism (i.e., the part which is independent of sample orientation and obeys both Lorentz reciprocity and directional reciprocity), linear dichroism, and linear birefringence, respectively. ACD produces the directionally nonreciprocal circular dichroism of the chiral thin film from the significant interference between linear birefringence (LB) and dichroic (LD) interactions (consequently, ACD is often referred to as "LDLB"). Here, we append a third term (LB_{res}) to allow for residual anisotropy, which stems from the inability to perform a "perfect" CD experiment due to technical limitations. In typical cases, this term results from residual birefringence from the photoelastic modulator in most CD spectrometers. In our experimental setup, the third term results from a similar occurrence caused by the dielectric coating on the coverslip HR mirrors (see below and SI).

To better understand the origins of the measured signals, we simulated angular spectra by solving Maxwell's equations within the Scattering Matrix Method (SMM) formalism [50] (full description in SI) using an augmented version of PyLlama [51]. Here, PTPO was first characterized using a combination of time-dependent density functional theory (TD-DFT) calculations alongside fitting of dipole parameters to solution and thin film spectra, Figures S6-S9. Since we observed CD at high angles in empty microcavities and stress often manifests in DBR manufacturing [52] we also implemented a full model of the microcavity including the DBR under shear strain, Figure S5, which accounts for the bandwidth response of the mirrors, deviations from ideal reflection in the mirrors, and the angle-dependent chiroptical response. Theoretical angular-resolved spectra (Figure 3d,e) yield excellent agreement with the experimental results for the PTPO-containing microcavities (Figure 3a,b). The major microcavity mode (Figure 3, major feature in all panels ~440 nm) is well-understood and reproduced theoretically. The minor peaks are highly susceptible to perturbations in microcavity mirror parameters such as mirror spacing, number of DBR periods, and DBR target wavelengths, and are only qualitatively approximated. Looking at the dispersion behavior, importantly, the increase in dissymmetry through the distinction between circularly-polarized modes of light at higher angles is captured by our model.

Spatial distribution of the CD signal

The PTPO films are not uniform samples, rather consisting of multiple crystalline domains of varying orientations [37]. Additional evidence of intrafilm diversity can be seen in time-resolved

fluorescence dynamics measured at multiple film locations, Figure S10. Each PTPO molecule consists of a centrosymmetric conjugated ring structure with two chiral oligomer side chains. Changing the handedness of the side chain changes the sign of the CD spectra [38], which can be interpreted as being due to the preferred orientation of the molecular assembly with respect to the substrate during spin coating. According to symmetry considerations, crystalline domains oriented with the same "face" of their conjugated ring to the substrate show an invariant ACD, but a flipping of orientation will result in a total inversion of the sign of the ACD signal. In conventional CD spectropolarimeters, the CD signal may result from the sum of multiple reinforcing or counteracting spatial domains (referred to as grains). However, in our setup, the light is focused to a spot size of diameter ~0.24 mm that is only slightly larger than the grain size [45], enabling measurement of a distribution of CD signals that varies as the contributions from different grains

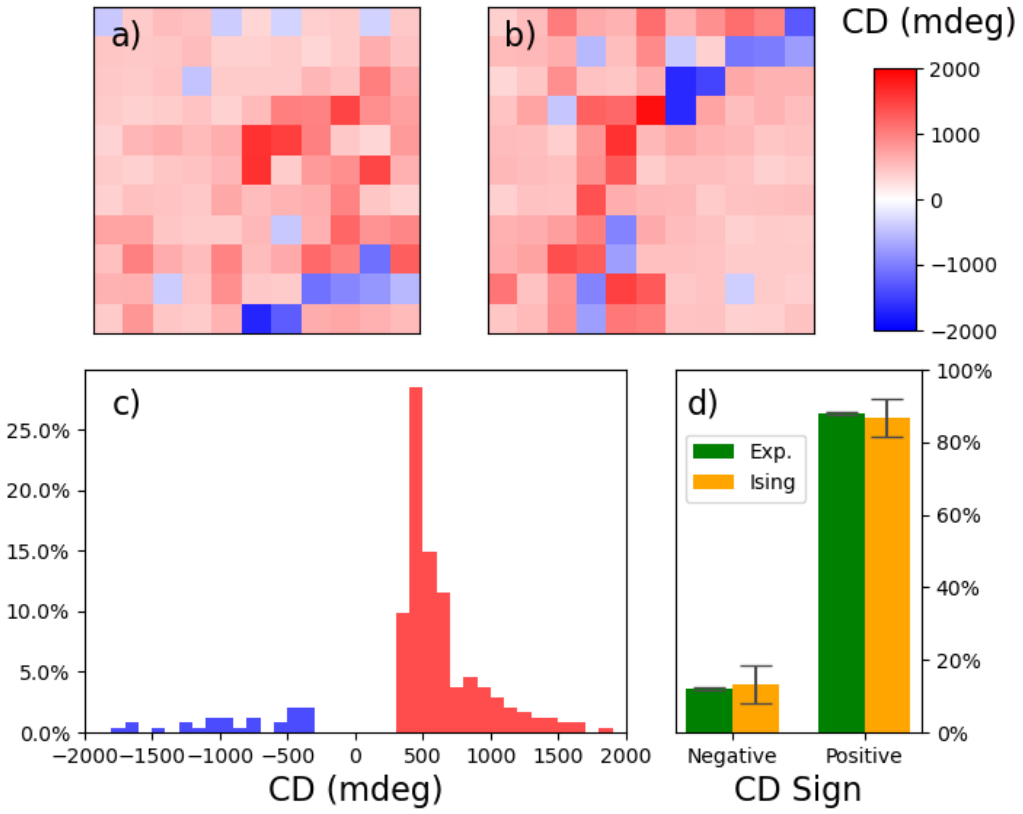

Figure 4. Spatial distribution of CD for microcavity containing PTPO 100 nm thin films. a-b) Spatial maps of CD with step size of 0.5 mm for two non-neighboring regions of PTPO. c) Histogram of CD for spatial maps depicted above (a,b). d) Distribution of positive and negative CD sign from c) compared with that for a Metropolis-Hastings simulation of an Ising model of two domain orientations. For the Ising model, CD sign given by averaging over 100 trajectories where the ratio between the substrate affinity per domain area of one orientation and the interdomain coupling per shared edge length is 2 mm (details in SI).

change. Figure 4a,b present 2D maps of CD value for a microcavity with 100 nm PTPO versus x-y position obtained by mapping a 10 by10 grid array area with a 0.5 mm step size.

A diversity of CD values at different spatial locations of the microcavity are observed, Figure 4c, including a dominant negative signal with regions of chiroptical signal inversion. This diversity is qualitatively similar to previous investigations of ACD-active oligothiophenes [45,53], but this imaging is accomplished with much thinner PTPO layers and without a high intensity synchrotron source due to the enhanced interaction length provided by the microcavity. The CD value consistently displays a magnitude above 300 mdeg, demonstrating that ACD exists regardless of precise grain composition. The largest magnitudes of CD nearly reach 2000 mdeg. As ACD results from the angle between microscopic LD and LB behavior for a single grain, it should be invariant to orientation of that grain within the *xy*-plane.

To understand why both signs of chiroptic response are observed, Monte Carlo simulations were performed on a modified Ising model of crystal domains (details in SI). Crystalline domains were approximated as a Voronoi tessellation [54] of the plane for which each domain could be orientated "face-up" or "face-down," with there being a favorable interaction between adjacent domains sharing orientation that is analogous to a ferromagnetic coupling (Ising model) and an overall bias towards one face that is analogous to an applied field. We implemented such a Voronoi-Ising model to obtain a steady-state distribution at temperatures near the critical temperature [55] (*38*). In doing so, we observe two equal and opposite values for CD (Figure 4d, yellow bars and Figure S11) with percentages comparable to what is obtained by averaging over the experimental results (Figure 4d, green bars). From such statistical mechanics, we are able to support our model that PTPO molecular domains preferentially but not perfectly orient in a particular direction. Ultimately, this thermodynamic effect in the production of the thin films produces a CD response that contains regions of dominant and minor polarity.

Discussion

The results above have demonstrated a new means of endowing Fabry-Pérot microcavities with an asymmetric chiral response using directionally nonreciprocal ACD, as well as using a microcavity to amplify the weak intrinsic chirality of a thin film. As ACD-active materials invert their chiroptic response with regards to light propagation direction, they enable symmetry breaking between chiral standing modes of a standard planar microcavity, while repeated round trips result in an enhancement of the chiral response by over an order of magnitude.

We reiterate that the PTPO-embedded microcavity contains both circular polarization modes propagating within it but that it preferentially absorbs RCP in one propagation direction and LCP in the other. While this phenomenon does not lend itself to uses that require helicity-preserving modes such as chiral sensing [56,57], it presents new opportunities for chiral engineering.

These new opportunities offer a variety of exciting applications. By placing molecules with specific electronic degeneracies into chiral cavities, polariton ring currents have been hypothesized to exist that can enhance CD signals [58]. By analogy to traditional resonator design, the chiral amplification of ACD-active cavities offers an alternative for chiral laser construction to

cholesteric liquid crystals [59] or chiral dyes [60]. An advantage of this method for chiral lasers would be the use of optimized standard mirrors to enhance optical gain and ultimately net helicity of output pulses. As ACD-active microcavities have a chiral response that inverts upon sample flipping and that preferentially transmits one circular polarization, they present a new means of producing polarization-dependent optical diodes [61,62] for quantum information processing [63] and the directional manipulation of light [64]. As ACD exhibits Lorentz reciprocity, its usage in engineering would create reciprocal diodes [65] that distinguish between polarization modes in contrast with complete optical isolators that block both modes and require nonreciprocity such as occurs via the Faraday effect [66]. Here, the explicit directionality of ACD would enable logical operations on photonic spin states in a controllable manner.

A clear goal for future research is the achievement of strong coupling in ACD-active cavities. Recently, a cavity quantum electrodynamical theory of ACD has predicted the generation of chiral polaritons arising when ACD samples are embedded in achiral FP cavities [67]. While the present work has not demonstrated splitting of polaritonic energies, this observation is hampered by the already broad spectral lineshapes of the PTPO. Co-incorporation of chromophores with sharper spectral features [68] in an additional material layer offers a clear path to this goal, and these experiments are in progress and represent a promising direction for future work.

All angle-dependent effects are invariant with respect to the sign of the incident angle. Concerning symmetry, the Lorentz-reciprocal, non-magnetic media in this study have a response that is necessarily symmetric under flipping the sign of the angle of incidence. Said another way, in the absence of magnetic effects, dielectric behavior must be the same for incident radiation of momentum at k_x or $-k_x$. As both strain-induced symmetric dielectric effects and ACD respect this symmetry, the optical behavior respects mirror symmetry about any plane perpendicular to the cavity. The phenomena discussed here therefore has fundamentally different symmetry considerations to the recently-observed chiral cavities from Gautier, Li, Ebbesen, and Genet [35]. In their recently-reported microcavities, the chiral vehicle is a torsionally-strained sheet illuminated at an oblique angle, which lacks the mirror symmetries of the ACD-active microcavities reported here and presents a predominantly flipped signal with respect to incident angle. Furthermore, we report access to a planar chirality with stronger helicity, particularly at normal incidence. At normal incidence, the largest CD values in our work reach 1800 mdeg, while the work of reference [35] demonstrate negligible CD values at normal incidence and a maximum signal of approximately 600 mdeg at highly oblique angles (this comparison further explained in SI). Our microcavities also demonstrate higher CD values at more oblique angles, but due the impact of LB_{res} terms at oblique angles due to strain of the HR substrate in our microcavities, we focus only the ACD-induced response at normal incidence [38]. The symmetry behavior observed in our investigation also differs with chiroptical behavior in systems such as monolayer transition metal dichalcogenides [69] or topologically-active Bloch modes [70] that invert in sign upon flipping either k_x or $-k_x$. The phenomena in ACD-active cavities should be understood in terms of the symmetry relations of reciprocal anisotropic media as opposed to gyroelectric, reciprocal magneto-electric, or non-reciprocal magneto-electric materials [16].

In this work, we have demonstrated a new means of enhancing the chiral response of directionally nonreciprocal ACD using planar microcavities. As ACD increases with pathlength, the repeated roundtrips of light enabled by the cavity finesse results in a magnification of CD values by 10-20x

for the 100 nm PTPO film at normal incidence, reaching extraordinary levels of dissymmetry for organic materials. Access to asymmetric chiroptic responses in microcavities at normal incidence will provide a powerful new photonic interface for quantum transduction.

Materials and Methods

Chiral thin film and microcavity preparation: The chiral thin films are composed of 3,3'-(2,5-bis(((S)-3,7- dimethyloctyl)oxy)-1,4-phenylene)bis(1-(thiophen-2-yl)prop-2-yn-1-one), also referred to as (S,S)-PTPO or PTPO, Figure 1c. The synthesis of PTPO was reported in Ref [38]. Highly reflective distributed Bragg reflector (DBR) mirrors, HRs, were purchased from Evaporated Coatings Inc (Willow Grove, PA, USA) with R=95% from 440-490nm (see SI). These HR substrates were washed first with acetone at 40°C, then isopropyl alcohol, then heated to 80°C. The HR substrates were then treated with an air plasma for surface activation. PTPO films were then spin-coated at 2000 rpm from dichloromethane PTPO solutions at conditions designed to create a 300 nm film (26 mg/mL), 100 nm film (3.25 mg/mL), or 50 nm film (1.2 mg/mL). Then the films underwent thermal annealing at 80 °C (compound melting point 95–97 °C).

To form a microcavity, a polyvinyl acetate (PVA, MW = 13,000-23,000, Sigma Aldrich) polymer adhesion layer of 100-160 nm (adjusted to ensure the cavity resonance is within the mirror coating regime) is spincoated (1700-2300 RPM, 50-60 mg/mL in chlorobenzene) on one HR using spin-coating. A PTPO thin film is deposited onto a second HR substrate according to the procedure above. The second HR is placed (film side down) on top of the first HR (polymer side up) in a home-built compression tool, and lamination is consequently achieved by compression at 12 MPa in an 80°C oven for 3h [47].

Experimental Setup for transmission circular dichroism: A fiber-coupled broadband white light source (SLS201L, Thorlabs) is collimated and directed through a Glan-Taylor linear polarizer and superachromatic quarter-wave plate (QWP, SAQWP05M-700, Thorlabs) to generate circularly polarized light. Rotating the QWP 90 degrees allows easy switching between RCP and LCP. The beam is then focused onto the sample via a lens with focal length 60 mm and transmitted light is recollimated and collected by a multimode fiber (FG200LEA, Thorlabs) connected to an optical spectrometer (Kymera 328i DV897ECS-BV, Andor). The spot size is measured with a CCD camera (Thorlabs, CS165CU/M).

The spectrometer records the transmission intensity for LCP and RCP excitation over a wavelength range of 380-500 nm wavelengths, then the CD is calculated for the entire spectrum according to Equation 1. The difference between LCP and RCP reflects the difference in chirality-specific absorption of the sample and is expected to be zero for achiral samples and chiral samples at non-absorbing wavelengths. The transmission spectrum for the HR mirrors at normal incidence serves as a background signal check to ensure that the transmission is equal for the LCP and RCP light. This check is performed to verify that the system is properly calibrated before taking measurements. By confirming the equality of transmission for LCP and RCP, we can ensure the accuracy of subsequent measurements and eliminate any potential systematic errors introduced by the instrument or setup.

Procedure for angle-dependent CD measurements: Microcavity samples are carefully mounted over the pivot point of a rotation stage (PR01, Thorlabs), which is itself mounted on a translation

stage used to center the sample (and pivot point) in the focus point of the beam and orthogonal to the propagation axis. The sample is rotated along an axis orthogonal to the propagation axis and LCP and RCP transmission spectra are recorded for different angles. The transmission intensities are then used to calculate the CD spectra according to Equation 1.

Procedure for 2D CD spatial maps: Microcavity samples are mounted on an XY translation stage in the focus point of the beam and orthogonal to the propagation axis. The sample is translated by 0.5 mm increments in x and y, maintaining the position along the propagation axis (z) and orthogonality to that axis (no angle of rotation). Transmission spectra for LCP and RCP are recorded for a 5x5mm square and used to calculate the CD spectra according to Equation 1.

Acknowledgments

Funding: Research was primarily supported as part of the Center for Molecular Quantum Transduction, an Energy Frontier Research Center funded by U.S. Department of Energy (DOE), Office of Science, Basic Energy Sciences (BES), under Award DE-SC0021314 (microcavity fabrication, characterization, and theory). In addition, LDB acknowledges support from PRIN 2017 project "CHIRALAB", grant number 20172M3K5N given by the Italian Ministry (MIUR) (PTPO synthesis), and MCA acknowledges support from the Air Force Office of Scientific Research award number FA9550-23-1-0181 (apparatus for sample preparation).

Author contributions:
Conceptualization: AS, FZ, GP, LDB, RG, RT, TC.
Funding acquisition: LDB, MA, MW, RG, RT
Investigation: AS, FU, JR, KP, PB, TC
Methodology: AD, AS, KP, JR, RG, RT, TC
Project administration: LDB, RG, RT
Data curation: AS, JR, KP, TC
Formal analysis: AS, KP, TC
Software: AS, KP, TC
Supervision: FZ, LDB, LAA, MA, MW, RG, RT
Visualization: AS, JR, KP, TC
Writing—original draft: AS, KP, PB, TC, RG
Writing---review & editing: AS, FZ, JR, GP, KP, LDB, RG, RT, TC

Competing interests: All authors declare they have no competing interests.

Data and materials availability: All data needed to evaluate the conclusions in the paper are present in the paper and/or the Supplementary Materials.

The authors thank Bart Kahr and Jonah Greenberg for discussions regarding the Berreman 4-by-4 matrix method and Monte Carlo simulations, respectively.

Citations:

1. Brandt, J. R., Salerno, F. & Fuchter, M. J. The added value of small-molecule chirality in technological applications. *Nat Rev Chem* **1**, 0045 (2017).
2. Huang, Y. *et al.* Room-temperature electron spin polarization exceeding 90% in an opto-spintronic semiconductor nanostructure via remote spin filtering. *Nat. Photonics* **15**, 475–482 (2021).
3. Mondal, P. C. *et al.* Chiral Conductive Polymers as Spin Filters. *Adv. Mater.* **27**, 1924–1927 (2015).
4. Yoo, S. & Park, Q.-H. Chiral Light-Matter Interaction in Optical Resonators. *Phys. Rev. Lett.* **114**, 203003 (2015).
5. Naaman, R., Paltiel, Y. & Waldeck, D. H. Chiral Induced Spin Selectivity Gives a New Twist on Spin-Control in Chemistry. *Acc. Chem. Res.* **53**, 2659–2667 (2020).
6. Aiello, C. D. *et al.* A Chirality-Based Quantum Leap. *ACS Nano* **16**, 4989–5035 (2022).
7. Lininger, A. *et al.* Chirality in Light–Matter Interaction. *Advanced Materials* 2107325 (2022) doi:10.1002/adma.202107325.
8. Sang, Y., Han, J., Zhao, T., Duan, P. & Liu, M. Circularly Polarized Luminescence in Nanoassemblies: Generation, Amplification, and Application. *Adv. Mater.* **32**, 1900110 (2020).
9. Du, W. *et al.* Strong Exciton–Photon Coupling and Lasing Behavior in All-Inorganic $CsPbBr_3$ Micro/Nanowire Fabry-Pérot Cavity. *ACS Photonics* **5**, 2051–2059 (2018).
10. Xiang, B. *et al.* Manipulating optical nonlinearities of molecular polaritons by delocalization. *Sci. Adv.* **5**, eaax5196 (2019).

11. Garcia-Vidal, F. J., Ciuti, C. & Ebbesen, T. W. Manipulating matter by strong coupling to vacuum fields. *Science* **373**, eabd0336 (2021).
12. Dunkelberger, A. D., Simpkins, B. S., Vurgaftman, I. & Owrutsky, J. C. Vibration-Cavity Polariton Chemistry and Dynamics. *Annu. Rev. Phys. Chem.* **73**, 429–451 (2022).
13. Wright, A. D., Nelson, J. C. & Weichman, M. L. Rovibrational Polaritons in Gas-Phase Methane. *J. Am. Chem. Soc.* **145**, 5982–5987 (2023).
14. Hübener, H. *et al.* Engineering quantum materials with chiral optical cavities. *Nat. Mater.* **20**, 438–442 (2021).
15. Salij, A. & Tempelaar, R. Microscopic theory of cavity-confined monolayer semiconductors: Polariton-induced valley relaxation and the prospect of enhancing and controlling valley pseudospin by chiral strong coupling. *Phys. Rev. B* **103**, 035431 (2021).
16. Khandekar, C., Khosravi, F., Li, Z. & Jacob, Z. New spin-resolved thermal radiation laws for nonreciprocal bianisotropic media. *New J. Phys.* **22**, 123005 (2020).
17. Barron, L. D. *Molecular Light Scattering and Optical Activity*. (Cambridge University Press, 2004).
18. Sofikitis, D. *et al.* Evanescent-wave and ambient chiral sensing by signal-reversing cavity ringdown polarimetry. *Nature* **514**, 76–79 (2014).
19. Vallet, M., Bretenaker, F., Le Floch, A., Le Naour, R. & Oger, M. The Malus Fabry–Perot interferometer. *Optics Communications* **168**, 423–443 (1999).
20. Müller, T., Wiberg, K. B. & Vaccaro, P. H. Cavity Ring-Down Polarimetry (CRDP): A New Scheme for Probing Circular Birefringence and Circular Dichroism in the Gas Phase. *J. Phys. Chem. A* **104**, 5959–5968 (2000).
21. Plum, E. & Zheludev, N. I. Chiral mirrors. *Appl. Phys. Lett.* **106**, 221901 (2015).

22. Kang, L. *et al.* Preserving Spin States upon Reflection: Linear and Nonlinear Responses of a Chiral Meta-Mirror. *Nano Lett.* **17**, 7102–7109 (2017).
23. Liu, W., Menon, V. M., Gao, S. & Agarwal, G. S. Chiral emission of electric dipoles coupled to optical hyperbolic materials. *Phys. Rev. B* **100**, 245428 (2019).
24. Solomon, M. L., Hu, J., Lawrence, M., García-Etxarri, A. & Dionne, J. A. Enantiospecific Optical Enhancement of Chiral Sensing and Separation with Dielectric Metasurfaces. *ACS Photonics* **6**, 43–49 (2019).
25. Zhang, X., Liu, Y., Han, J., Kivshar, Y. & Song, Q. Chiral emission from resonant metasurfaces. *Science* **377**, 1215–1218 (2022).
26. Zhao, Y. *et al.* Nanoscopic control and quantification of enantioselective optical forces. *Nature Nanotech* **12**, 1055–1059 (2017).
27. Solomon, M. L. *et al.* Nanophotonic Platforms for Chiral Sensing and Separation. *Acc. Chem. Res.* **53**, 588–598 (2020).
28. Kim, J. *et al.* Induction and control of supramolecular chirality by light in self-assembled helical nanostructures. *Nat Commun* **6**, 6959 (2015).
29. Kumar, J. & Liz-Marzán, L. M. Recent Advances in Chiral Plasmonics — Towards Biomedical Applications. *BCSJ* **92**, 30–37 (2019).
30. Zhang, Q. *et al.* Unraveling the origin of chirality from plasmonic nanoparticle-protein complexes. *Science* **365**, 1475–1478 (2019).
31. Lee, Y. Y., Kim, R. M., Im, S. W., Balamurugan, M. & Nam, K. T. Plasmonic metamaterials for chiral sensing applications. *Nanoscale* **12**, 58–66 (2020).
32. Kim, J. W. *et al.* Controlling the size and circular dichroism of chiral gold helicoids. *Mater. Adv.* **2**, 6988–6995 (2021).

33. Vila-Liarte, D., Kotov, N. A. & Liz-Marzán, L. M. Template-assisted self-assembly of achiral plasmonic nanoparticles into chiral structures. *Chem. Sci.* **13**, 595–610 (2022).
34. Cai, J. *et al.* Polarization-sensitive optoionic membranes from chiral plasmonic nanoparticles. *Nat. Nanotechnol.* **17**, 408–416 (2022).
35. Gautier, J., Li, M., Ebbesen, T. W. & Genet, C. Planar Chirality and Optical Spin–Orbit Coupling for Chiral Fabry–Perot Cavities. *ACS Photonics* **9**, 778–783 (2022).
36. Albano, G., Pescitelli, G. & Di Bari, L. Chiroptical Properties in Thin Films of π-Conjugated Systems. *Chem. Rev.* **120**, 10145–10243 (2020).
37. Albano, G. *et al.* Outstanding Chiroptical Features of Thin Films of Chiral Oligothiophenes. *ChemNanoMat* **4**, 1059–1070 (2018).
38. Zinna, F. *et al.* Emergent Nonreciprocal Circularly Polarized Emission from an Organic Thin Film. *Adv. Mater.* **32**, 2002575 (2020).
39. Disch, R. L. & Sverdlik, D. I. Apparent circular dichroism of oriented systems. *Anal. Chem.* **41**, 82–86 (1969).
40. Kuroda, R., Harada, T. & Shindo, Y. A solid-state dedicated circular dichroism spectrophotometer: Development and application. *Review of Scientific Instruments* **72**, 3802–3810 (2001).
41. Salij, A., Goldsmith, R. H. & Tempelaar, R. Theory of Apparent Circular Dichroism Reveals the Origin of Inverted and Noninverted Chiroptical Response under Sample Flipping. *J. Am. Chem. Soc.* **143**, 21519–21531 (2021).
42. Lindorfer, D. & Renger, T. Theory of Anisotropic Circular Dichroism of Excitonically Coupled Systems: Application to the Baseplate of Green Sulfur Bacteria. *J. Phys. Chem. B* **122**, 2747–2756 (2018).

43. Górecki, M. *et al.* Electronic Circular Dichroism Imaging (ECDi) Casts a New Light on the Origin of Solid-State Chiroptical Properties. *Chemistry A European J* **28**, (2022).
44. Berova, N., Bari, L. D. & Pescitelli, G. Application of electronic circular dichroism in configurational and conformational analysis of organic compounds. *Chem. Soc. Rev.* **36**, 914 (2007).
45. Albano, G. *et al.* Electronic circular dichroism imaging (CDi) maps local aggregation modes in thin films of chiral oligothiophenes. *New J. Chem.* **43**, 14584–14593 (2019).
46. Ismail, N., Kores, C. C., Geskus, D. & Pollnau, M. Fabry-Pérot resonator: spectral line shapes, generic and related Airy distributions, linewidths, finesses, and performance at low or frequency-dependent reflectivity. *Opt. Express* **24**, 16366 (2016).
47. Dhavamani, A., Haeberlé, L., Wang, J., Kéna-Cohen, S. & Arnold, M. S. Cavity-Mediated Hybridization of Bright and Dark Excitons in an Ultrastrongly Coupled Carbon Nanotube Microcavity. *ACS Photonics* **8**, 2375–2383 (2021).
48. Ribeiro, R. F., Martínez-Martínez, L. A., Du, M., Campos-Gonzalez-Angulo, J. & Yuen-Zhou, J. Polariton chemistry: controlling molecular dynamics with optical cavities. *Chem. Sci.* **9**, 6325–6339 (2018).
49. Torres, J. P., Hendrych, M. & Valencia, A. Angular dispersion: an enabling tool in nonlinear and quantum optics. *Adv. Opt. Photon.* **2**, 319 (2010).
50. Ko, D. Y. K. & Sambles, J. R. Scattering matrix method for propagation of radiation in stratified media: attenuated total reflection studies of liquid crystals. *J. Opt. Soc. Am. A* **5**, 1863 (1988).

51. Bay, M. M., Vignolini, S. & Vynck, K. PyLlama: A stable and versatile Python toolkit for the electromagnetic modelling of multilayered anisotropic media. *Computer Physics Communications* **273**, 108256 (2022).
52. Breiland, W. G., Allerman, A. A., Klem, J. F. & Waldrip, K. E. Distributed Bragg Reflectors for Vertical-Cavity Surface-Emitting Lasers. *MRS Bull.* **27**, 520–524 (2002).
53. Albano, G. *et al.* Spatially resolved chiroptical study of thin films of benzo[1,2-b:4,5-b']dithiophene-based oligothiophenes by synchrotron radiation electronic circular dichroism imaging (SR-ECDi) technique. *Aggregate* **3**, (2022).
54. Lima, F. W. S., Moreira, J. E., Andrade, J. S. & Costa, U. M. S. The ferromagnetic Ising model on a Voronoi–Delaunay lattice. *Physica A: Statistical Mechanics and its Applications* **283**, 100–106 (2000).
55. Bedanov, V. M. & Peeters, F. M. Ordering and phase transitions of charged particles in a classical finite two-dimensional system. *Phys. Rev. B* **49**, 2667–2676 (1994).
56. Feis, J. *et al.* Helicity-Preserving Optical Cavity Modes for Enhanced Sensing of Chiral Molecules. *Phys. Rev. Lett.* **124**, 033201 (2020).
57. Bao, J. *et al.* Chirality Enhancement Using Fabry–Pérot-Like Cavity. *Research* **2020**, 2020/7873581 (2020).
58. Sun, S., Gu, B. & Mukamel, S. Polariton ring currents and circular dichroism of Mg-porphyrin in a chiral cavity. *Chem. Sci.* **13**, 1037–1048 (2022).
59. Qu, D., Archimi, M., Camposeo, A., Pisignano, D. & Zussman, E. Circularly Polarized Laser with Chiral Nematic Cellulose Nanocrystal Cavity. *ACS Nano* **15**, 8753–8760 (2021).
60. Jiménez, J. *et al.* Chiral Organic Dyes Endowed with Circularly Polarized Laser Emission. *J. Phys. Chem. C* **121**, 5287–5292 (2017).

61. Gevorgyan, A. H. & Harutyunyan, M. Z. Chiral photonic crystals with an anisotropic defect layer. *Phys. Rev. E* **76**, 031701 (2007).

62. Söllner, I. *et al.* Deterministic photon–emitter coupling in chiral photonic circuits. *Nature Nanotech* **10**, 775–778 (2015).

63. Duan, L.-M. & Kimble, H. J. Scalable Photonic Quantum Computation through Cavity-Assisted Interactions. *Phys. Rev. Lett.* **92**, 127902 (2004).

64. Neugebauer, M., Bauer, T., Banzer, P. & Leuchs, G. Polarization Tailored Light Driven Directional Optical Nanobeacon. *Nano Lett.* **14**, 2546–2551 (2014).

65. Li, J., Ye, H., Yu, Z. & Liu, Y. Design of a broadband reciprocal optical diode in a silicon waveguide assisted by silver surface plasmonic splitter. *Opt. Express* **25**, 19129 (2017).

66. Jalas, D. *et al.* What is — and what is not — an optical isolator. *Nature Photon* **7**, 579–582 (2013).

67. Salij, A. H., Goldsmith, R. H. & Tempelaar, R. Chiral polaritons based on achiral Fabry–Pérot cavities using apparent circular dichroism. *arXiv:2208.14461v2* 14 (2022).

68. Ebbesen, T. W. Hybrid Light–Matter States in a Molecular and Material Science Perspective. *Acc. Chem. Res.* **49**, 2403–2412 (2016).

69. Caruso, F., Schebek, M., Pan, Y., Vona, C. & Draxl, C. Chirality of Valley Excitons in Monolayer Transition-Metal Dichalcogenides. *J. Phys. Chem. Lett.* **13**, 5894–5899 (2022).

70. Zeng, Y., Hu, G., Liu, K., Tang, Z. & Qiu, C.-W. Dynamics of Topological Polarization Singularity in Momentum Space. *Phys. Rev. Lett.* **127**, 176101 (2021).